

Electronic Supplementary Information (ESI)

Nitrogen-Doped Carbon Nanosheets and Nanoflowers with Holey Mesopores for Efficient Oxygen Reduction Catalysis

Hao Tian^a, Nan Wang^a, Fugui Xu^a, Pengfei Zhang^a, Dan Hou^a, Yiyong Mai^{a}, and Xinliang Feng^b*

^a School of Chemistry and Chemical Engineering, Shanghai Key Laboratory of Electrical Insulation and Thermal Ageing, Shanghai Jiao Tong University, 800 Dongchuan RD, Shanghai 200240, China

^b Department of Chemistry and Food Chemistry, Technische Universität Dresden, Mommsenstrasse 4, 01062 Dresden, Germany

E-mail: mai@sjtu.edu.cn

1. Experimental section

1.1 Chemicals and reagents

Monomethoxy poly (ethylene oxide) (monomethoxy-PEO5000), CuBr, triethylamine, 2-bromoisobutyrylbromide, bipyridine, styrene, and toluene were purchased from Sigma-Aldrich. Methanol, ether, anhydrous ethanol, tetrahydrofuran (THF), m-phenylenediamine and ammonium persulfate (APS) were purchased from Sinopharm Chemical Reagent Co. Ltd. Other chemicals were purchased from Aladdin Reagent (Shanghai) and used without further purification.

1.2 Materials preparation

1.2.1 Synthesis of PS-*b*-PEO copolymer

The PS-*b*-PEO diblock copolymer was prepared by a living ATRP method, including two steps.¹ The first step involved the synthesis of macroinitiator PEO₁₁₄-Br. according to the reported procedures. In the second step, 2g PEO₁₁₄-Br macroinitiator (3.8×10^{-3} mol) was placed in a 200 mL two-neck schlenk flask equipped with a septum. Then, 0.034g CuBr (2.4×10^{-3} mol) along with 0.11g bipyridine (1.5×10^{-2} mol) were added and the flask was evacuated and refilled with N₂ in several cycles in order to remove the oxygen. In a separate schlenk tube, 6 mL (3.5×10^{-2} mol) freshly distilled styrene was deoxygenated by bubbling N₂ gas for at least 0.5 hour. The styrene was then transferred to the macroinitiator flask via a double-tipped needle; the resulting dark-brown mixture was stirred at room temperature for 10 minutes and further deoxygenated by three freeze-and-thaw cycles. The mixture was cooled to room temperature and then placed in a thermostated oil-bath with a temperature of 120 °C, followed by stirring for 6 hours. The polymerization was quenched by the addition of a large amount of THF solvent and exposure to air. The mixture was passed through a short column of basic alumina and then precipitated into a large excess of methanol. The precipitate was filtered and then washed with methanol. The final product was dried under vacuum at 40 °C for 2 days.

1.2.2 Preparation of the layered double hydroxides (LDH) template.

LDH nanosheets were prepared according to a modified method.² Typically, 3.5 mmol cobalt chloride, 1.75 mmol nickel chloride, 0.35 mmol polyvinyl pyrrolidone (PVP, $M_w = 15000$) and 31.5 mmol hexamethylenetetramine (HMT) were dissolved in 700 mL deionized

water. The solution was refluxed for 5 h under continuous magnetic stirring and nitrogen protection. The precipitate was obtained by filtration, washing with deionized water and anhydrous ethanol for over three times, and finally air-drying at room temperature.

LDH nanoflowers were prepared according to the reported procedures.³ Typically, 3.5 mmol nickel nitrate, 1.75 mmol manganese chloride and 31.5 mmol hexamethylenetetramine (HMT) were dissolved in 700 mL deionized water. The solution was treatment at 80°C for 10 h. The precipitate was obtained by filtration, washing with deionized water and anhydrous ethanol for over 3 times, followed by air-drying at room temperature.

1.2.3 Preparation of N-doped mesoporous hexagonal carbon nanosheets (NMHCSs)

Typically, 0.06 g PS-*b*-PEO copolymer was dissolved in a mixture of 12 mL THF, 12 mL ethanol and 24 mL H₂O to generate the micellar aggregation. Then, 120 mg LDH nanosheets and 80 mg mPD were added to the solution. After 1 hour mild stirring of the mixed solution, 20 mL aqueous solution of ammonium persulfate (APS) (concentration: 20 mg/mL) was slowly added into the mixed solution to initiate the polymerization of mPD and the reaction was continued for 24 h. The product was collected and purified by centrifugation and washing with ethanol and water for at least 3 cycles. Finally, the collected product was air-dried at 40 °C for 12 h to yield PS-*b*-PEO/PmPD nanocomposite. Carbonization of the composite was carried out under nitrogen atmosphere at 800 °C for 2 h with a heating rate of 2 °C min⁻¹. The control sample, NCSs, was prepared under the similar experimental conditions excluding the addition of the copolymer template.

1.2.4 Preparation of N-doped mesoporous carbon nanoflowers (NMCFs)

The synthesis of NMCFs followed a procedure similar to that applied to NMHCSs, except the use of the LDH nanoflowers as the template.

1.2.5 Characterizations and measurements

¹H NMR spectrum was recorded on a Mercury Plus 400 (400 MHz for proton)

spectrometer with tetramethylsilane as the internal standard. Gel permeation chromatography (GPC) was operated on a Shimadzu Prominence system with a refractive index detector (Shimadzu RID-10A) at 40 °C, using THF as the eluent and polystyrene (PS) as the standard. Scanning electron microscopy (SEM) observations were performed on a FEI Sirion-200 (FEI Co., USA) field emission scanning electron microscope at 10 kV. The samples were dispersed in water by sonication and then dropped onto silicon wafers, followed by air-drying at ambient temperature at ambient temperature. Transmission electron microscopy (TEM) measurements were performed on a JEOL-2100(JEOL Ltd., Japan) at an accelerating voltage of 200 kV. All the samples for TEM measure were suspended in deionized water and drop-cast onto copper grids covered with carbon films, followed by air-drying at ambient temperature. X-Ray photoelectron spectroscopy (XPS) was conducted on an AXIS Ultra DLD system (Kratos Co., Japan) with Al K α radiation as the X-ray source. All the binding energies were calibrated via referencing to C1s binding energy (284.6 eV). Nitrogen adsorption isotherms were obtained on an Autosorb-iQA3200-4 sorption analyzer (Quantatech Co., USA) instrument at 77K. Before measurement, samples were degassed in a vacuum at 150 °C for at least six hours. Brunauer-Emmett-Teller (BET) method was utilized to calculate the specific surface area using adsorption data in a relative pressure range from 0.06 to 0.2. The pore size distributions were derived from the adsorption branches of isotherms using Barrett-Joyner-Halenda (BJH) method. Raman spectroscopy was conducted on an Invia/Reflrx Laser Micro-Raman spectrometer (Renishaw, England) excited by a laser beam of 532 nm. Powder XRD patterns were recorded on a Rigaku X-ray diffractometer D/MAX-2200/PC with Cu K α radiation ($\lambda = 0.154$ nm) at a scan rate of 0.6 ° min⁻¹ over the 2 θ range of 5-80 °. Fourier-transform infrared spectra between 4,000 and 400 cm⁻¹ were recorded using a Nicolet iS10. Atomic Force Microscopy (AFM) images were recorded on a scanning probe microscope (Multimode Nanoscope, USA) operated via tapping mode by using silicon nitride cantilevers with a force constant of 0.12 N/m. Inductively coupled plasma atomic emission spectrometry (ICP-AES) was performed on a Thermo Fisher iCAP7600 spectrometer.

1.2.6 Electrochemical measurements.

The ORR performance was evaluated on an electrochemical workstation (Pine Instrument

Co., Ltd., USA). The potential difference between Ag/AgCl and reversible hydrogen electrode (RHE) was calculated to be 0.944 V. The working electrode was prepared as follows: 2 mg sample was dispersed in a 500 μL Nafion ethanol solution (0.25wt %) and then the resultant dispersion was sonicated for 0.5 h to achieve a homogeneous ink. Next, 9 μL of the dispersion was dropped on polished glassy carbon electrode with a loading of 0.24 mg cm^{-2} and then air-dried at room temperature. CV curves were measured in a N_2 - or O_2 -saturated basic media (0.1 M KOH) from -1 - 0 V vs. Ag/AgCl with a sweep rate of 100 mV s^{-1} . RDE was measured in O_2 -saturated 0.1M KOH from -1 - 0.2V vs. Ag/AgCl with different disk rotation rates of 400–2025 rpm at a sweep rate of 10 mV s^{-1} . Rotating ring disk electrode (RRDE) curves were recorded in O_2 -saturated 0.1M KOH at 1600 rpm at a scan rate of 10 mV/s . The chronoamperometric response was tested at 0.5V in O_2 -saturated 0.1 M KOH at 1600 rpm.

The electron transfer number (n) and the H_2O_2 yield were determined by the following equations:⁴

$$n = 4 \times I_{\text{D}} / (I_{\text{R}} / N + I_{\text{D}});$$

$$\text{H}_2\text{O}_2 \% = 200 \times I_{\text{R}} / N / (I_{\text{R}} / N + I_{\text{D}});$$

where I_{D} and I_{R} refer to disk current and ring current, respectively; and $N=0.37$ is the ring collection.

The electron transfer number (n) per oxygen molecule in an ORR process could also be calculated by the Koutecky–Levich (K–L) equations

$$J^{-1} = J_{\text{L}}^{-1} + J_{\text{K}}^{-1} = B^{-1} \omega^{-1/2} + J_{\text{K}}^{-1};$$

$$B = 0.2nFC_0(D_0)^{2/3} \nu^{-1/6}$$

J is the measured current density; J_{K} and J_{L} are the kinetic- and diffusion-limiting current densities, respectively; ω denotes the angular velocity of the disk; n represents the overall number of electrons transferred in oxygen reduction; F expresses the Faraday constant ($F = 96485 \text{ C mol}^{-1}$); C_0 is the bulk concentration of O_2 ; ν denotes the kinematic viscosity of the electrolyte, and k stands for the electrontransfer rate constant. The number of electrons transferred (n) can be obtained from the slope of the Koutecky-Levich plots. The constant is 0.2, when the rotating speed is in rpm.

The stability and resistance to the methanol crossover effect were tested by using the same setup as for the RDE test at a static potential of -0.3 V and -0.5 V , respectively, for

chronoamperometry at room temperature.

2. Figures and Tables

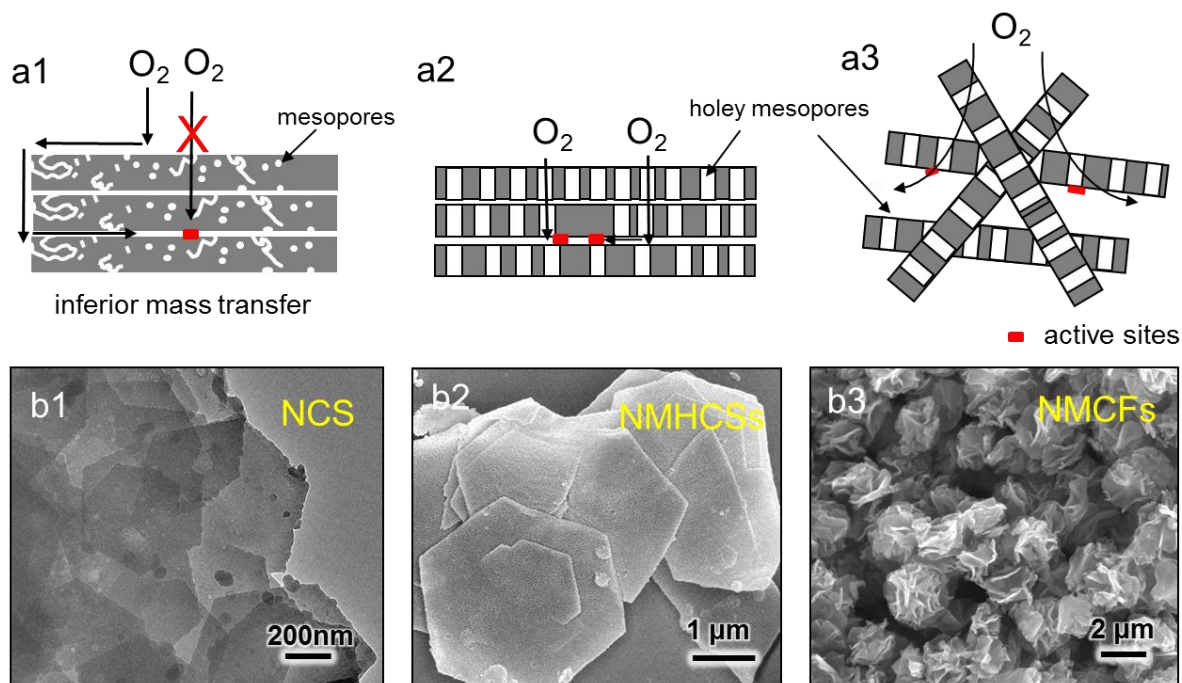


Figure S1. Schematic illustrations of the preferential layer-by-layer stacking of mesoporous nanosheets without holey pores (a1) and with holey pores (a2), as well as the 3D packing of mesoporous nanosheets with holey pores (a3). In the illustrations, the different diffusion pathways of O_2 molecules to the active sites buried in the interior of stacking space are shown. (b1-b3) Representative TEM images of NCSs (b1), NMHCSs (b2) and NMCFs (b3).

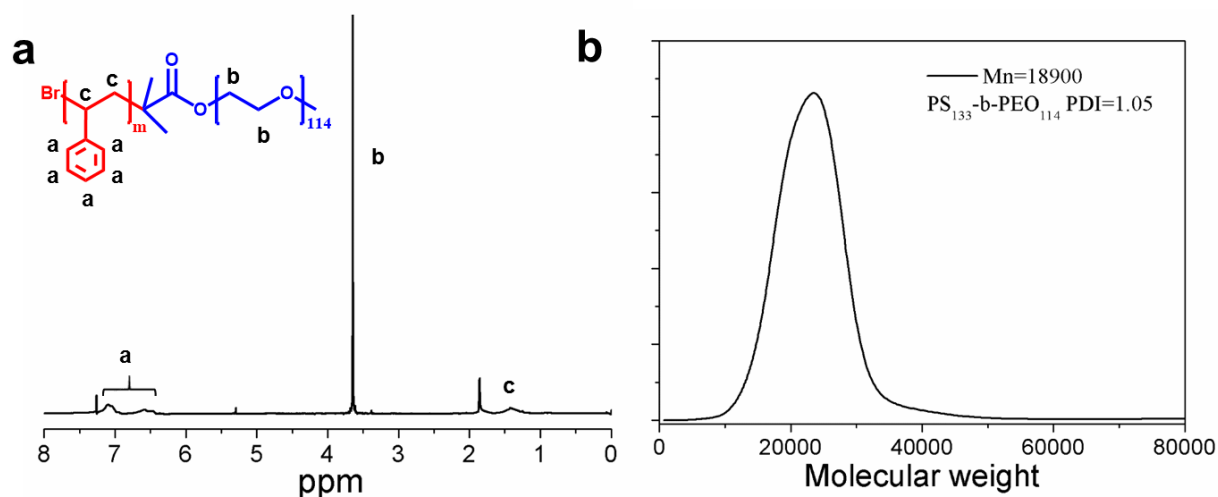


Figure S2. ^1H NMR spectrum (a) and GPC curve (b) of $\text{PS}_{133}\text{-}b\text{-PEO}_{114}$

From the NMR spectrum, the degree of polymerization (DP) of PS can be calculated as follows:

$$DP_{ps} = \frac{I_a / 5}{I_b / 4} \times 114 \approx 125$$

In the equation, I_a is the integrated value of the proton peaks attributed to phenyl groups of PS block (signal **a**), I_b represents the integrated value of the proton peaks attributed to PEO block (signal **b**). 114 is the DP of the PEO block.

DP_{ps} of PS-*b*-PEO calculated from GPC (Figure S2b) is 133, which is in good agreement with the NMR result. Accordingly, we refer to the GPC result for the DP of the PS block.

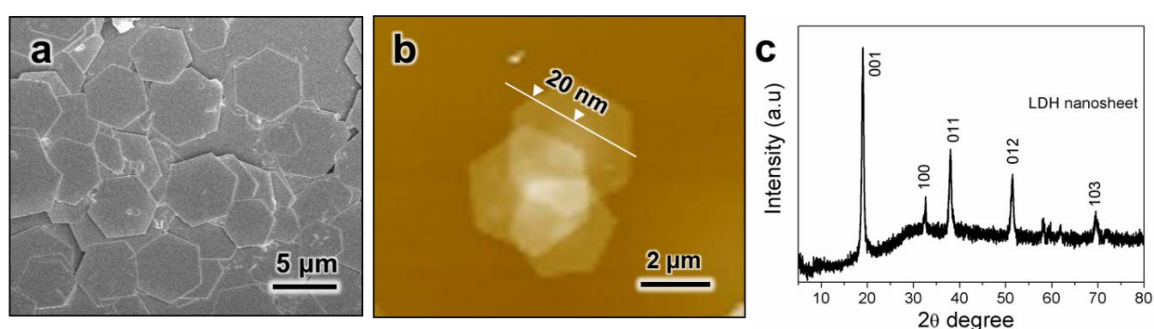


Figure S3. Structural characterizations of the $\text{Co}^{2+}\text{-Ni}^{2+}$ derived LDH nanosheets. (a) SEM image, (b) AFM height profile, (c) XRD pattern.

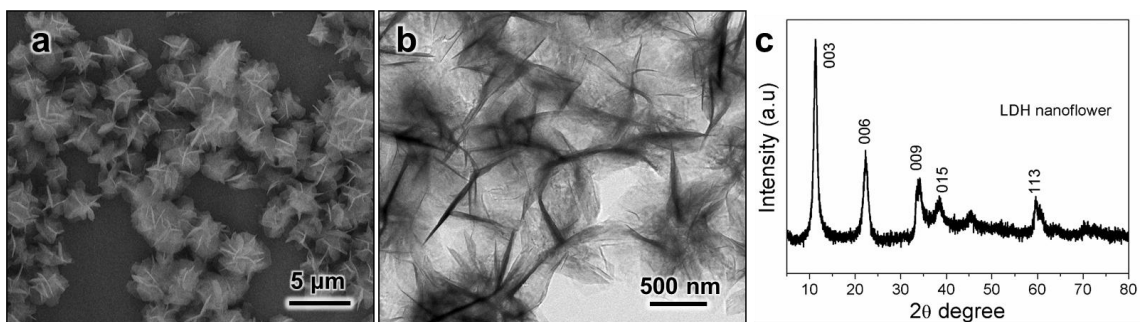


Figure S4. Structural characterization of the Ni²⁺-Mn³⁺ derived LDH nanoflowers. (a) SEM image, (b) TEM image (c) XRD pattern.

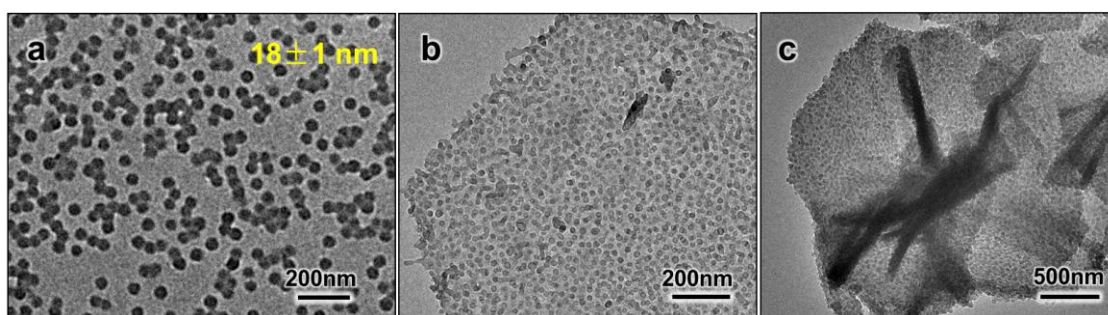


Figure S5. TEM image of the PS₁₃₃-*b*-PEO₁₁₄ micelles (a), the LDH nanosheets with spherical micelles closely-packed on the surfaces (b), and the LDH nanoflowers with spherical micelles closely-packed on the surfaces (c).

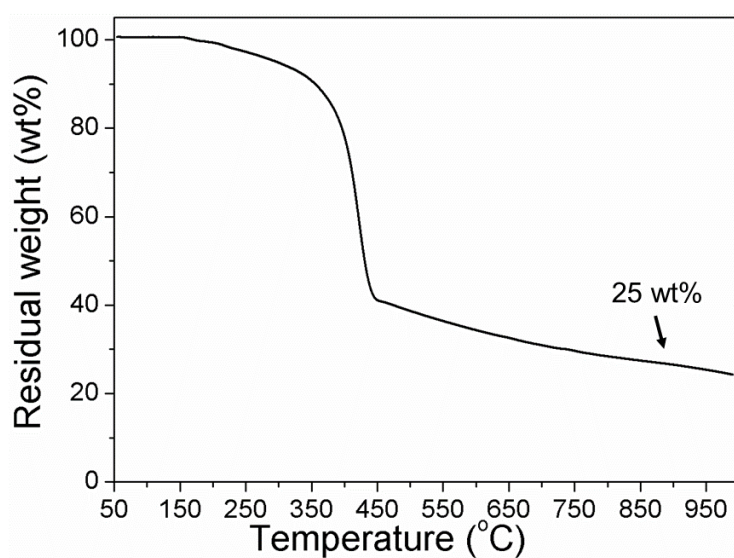


Figure S6. TGA curve of the PS₁₃₃-*b*-PEO₁₁₄/PmPD nanocomposite

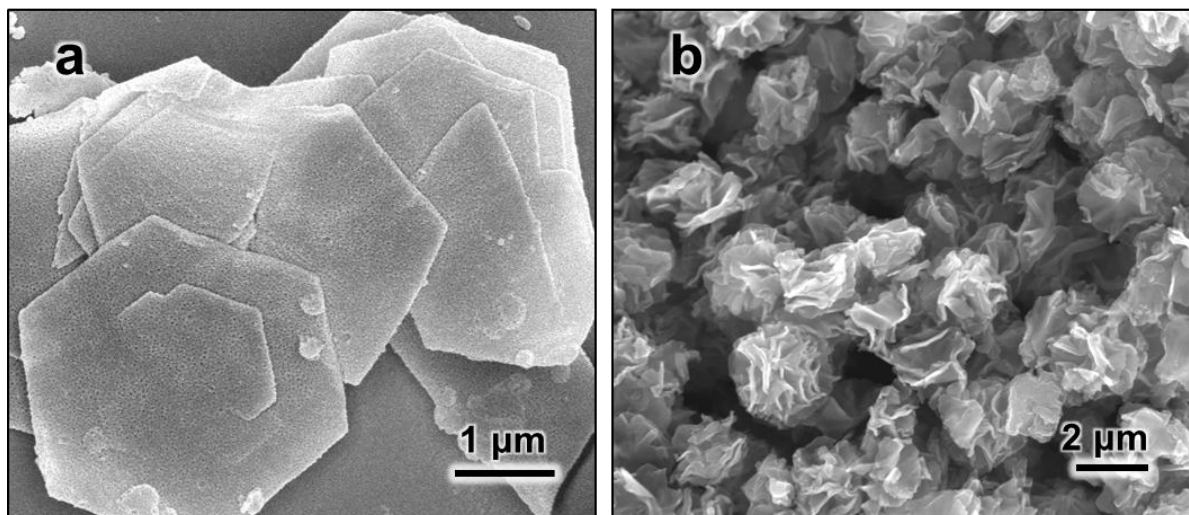


Figure S7. Typical SEM images of NMHCSs (a) and NMCFs (b)

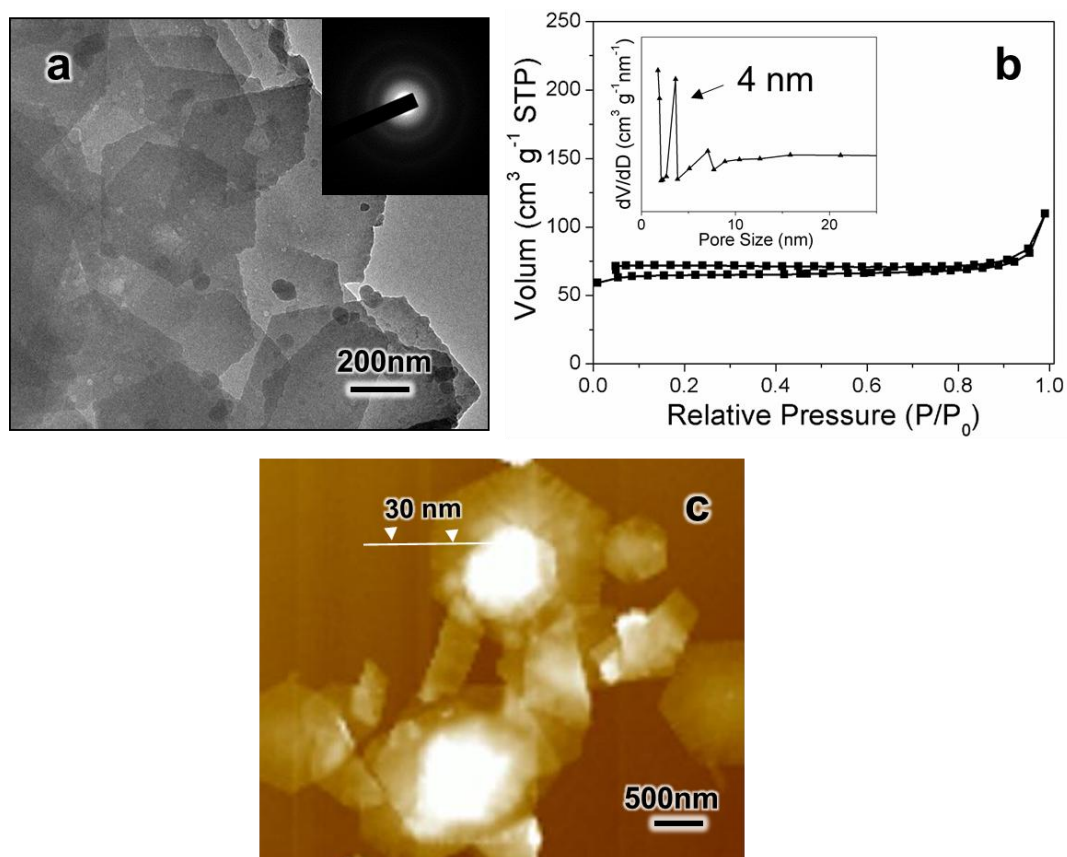


Figure S8. Structural characterizations of NCSs. (a) TEM image, the inset shows the SEAD pattern. (b) Nitrogen adsorption–desorption isotherm, the inset shows the pore size distribution. (c) AFM height profile.

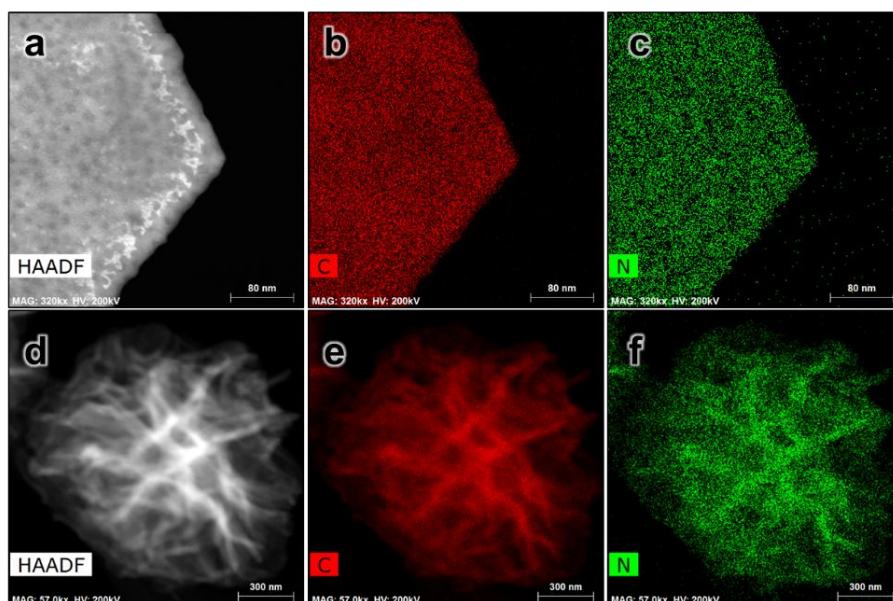


Figure S9. HAADF-STEM images and the corresponding element mapping of NMHCSs (a, b, c) and NMCFs (d, e, f).

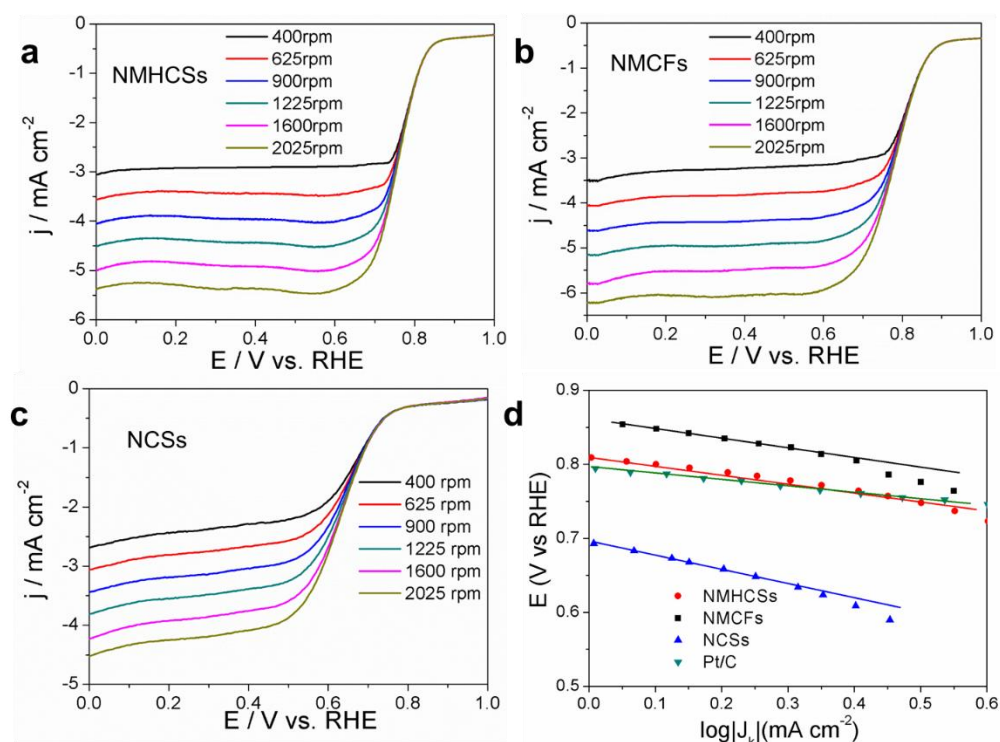


Figure S10. LSV plots of NMHCSs (a), NMCFs (b) and NCSs (c) in an O_2 -saturated 0.1 M KOH solution at a scan rate of 10 mV s^{-1} and different rotation speeds. (d) Tafel plots of NMHCSs, NMCFs, NCSs and Pt/C catalysts.

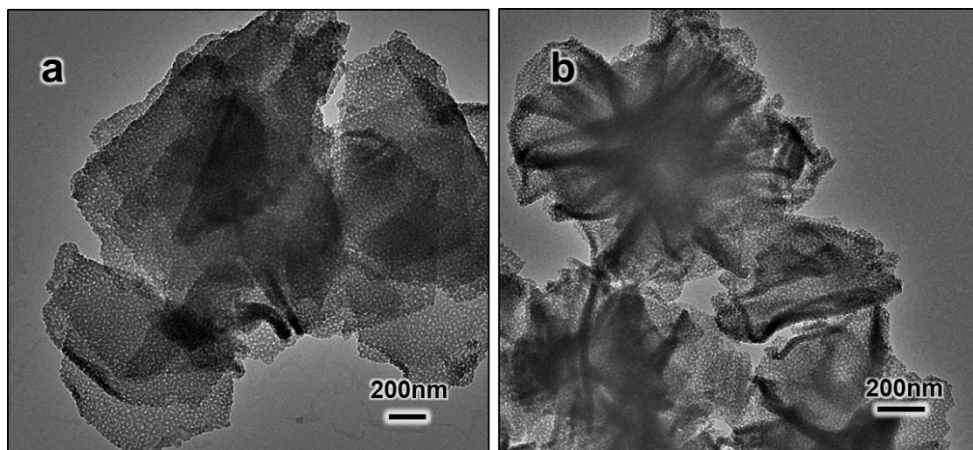


Figure S11. TEM images of NMHCSs (a) and NMCFs (b) after the testing of their ORR catalytic activity.

Table S1. Comparison of the ORR performance of our nitrogen-doped holey mesoporous carbon nanomaterials with those of some reported nitrogen-doped 2D carbon catalysts.

Sample names	Specific Surface Area ($\text{m}^2 \text{g}^{-1}$)	Electrolyte	Half-wave-potential (V vs RHE)	Limiting current density (mA cm^{-2})	Literature
NMCFs	266	0.1M KOH	0.80	5.5	This work
NMHCSs	256	0.1M KOH	0.77	5.0	This work
Nitrogen-doped carbon/rGO nanosheets	589	0.1M KOH	0.79	5.0	Ref. 5
Nitrogen-doped porous graphene	806	0.1M KOH	0.75	4.5	Ref. 6
Nitrogen-doped sheet-like porous carbon	515	0.1M KOH	0.70	4.6	Ref. 7
Nitrogen-doped nanoporous carbon nanosheets	646	0.1M KOH	0.74	4.7	Ref. 8
Nitrogen-doped mesoporous carbon /rGO sandwiches	339	0.1M KOH	0.60	3.4	Ref. 9
Nitrogen-doped mesoporous carbon/rGO nanosheets	374	0.1M KOH	0.72	3.8	Ref. 10
Nitrogen-doped graphene	750	0.1M KOH	0.73	4.6	Ref. 11
Microporous carbon/rGO nanosheet	681	0.1M KOH	0.71	4.0	Ref. 12
Nanoporous nitrogen-doped graphene	377	0.1M KOH	0.69	4.3	Ref. 13
Nitrogen-doped graphene	350	0.1M KOH	0.57	3.4	Ref. 14

For the convenience of comparison, the measure potentials vs Ag/AgCl were converted to a reversible hydrogen electrode (RHE) scale according to the Nerst equation ($E_{\text{RHE}} = E_{\text{Ag/AgCl}} + 0.059 \times \text{pH} + 0.198$).

Reference

1. Y. Y. Mai, A. Eisenberg, *J. Am. Chem. Soc.* **2010**, 132, 10078.
2. J. B. Liang, R. Z. Ma, N. Iyi, Y. Ebina, K. Takada, T. Sasaki, *Chem. Mater.* **2010**, 22, 371.
3. J. W. Chen, X. Wang, J. X. Wang, P. S. Lee, *Adv. Energ. Mater.* **2016**, 6, 1745.
4. G. Wang, Y. H. Sun, D. B. Li, H. W. Liang, R. H. Dong, X. L. Feng, K. Müllen, *Angew. Chem. In. Ed.* **2015**, 127, 15406.
5. W. Wei, H. W. Liang, K. Parvez, X. D. Zhuang, X. L. Feng, K. Müllen, *Angew. Chem. In. Ed.* **2014**, 126, 1596.
6. L. Qin, R. M. Ding, H. X. Wang, J. H. Wu, C. H. Wang, C. H. Zhang, Y. Xu, L. C. Wang, B. L. Lv, *Nano Research* **2017**, 10, 305.
7. P. Zhang, F. Sun, Z. H. Xiang, Z. G. Shen, J. Yun, D. P. Cao, *Energ. Environ. Sci.* **2014**, 7, 442.
8. P. Chen, L. K. Wang, G. Wang, M. R. Gao, J. Ge, W. J. Yuan, Y. H. Shen, A. J. Xie, S. H. Yu, *Energ. Environ. Sci.* **2014**, 7, 4095.
9. M. Qiao, C. Tang, G. He, K. Qiu, R. Binions, I. P. Parkin, Q. Zhang, Z. Guo, M. M. Titirici, *J. Mater. Chem. A* **2016**, 4, 12658.
10. K. G. Qu, Y. Zheng, S. Dai, S. Z. Qiao, *Nanoscale* **2015**, 7, 12598.
11. J. J. Li, Y. M. Zhang, X. H. Zhang, J. C. Han, Y. Wang, L. Gu, Z. H. Zhang, X. J. Wang, J. K. Jian, P. Xu, B. Song, *ACS Applied Mater. & Inter.* **2015**, 7, 19626.
12. X. D. Zhuang, F. Zhang, D. Q. Wu, N. Forler, H. W. Liang, M. Wagner, D. Gehrig, M. R. Hansen, F. Laquai, X. L. Feng, *Angew. Chem. In. Ed.* **2013**, 52, 9668.
13. Z. Y. Lin, G. H. Waller, Y. Liu, M. L. Liu, C. P. Wong, *Carbon* **2013**, 53, 130.
14. S. Yasuda, L. Yu, J. Kim, K. Murakoshi, *Chem. Commun.* **2013**, 49, 9627.